Fracture Mechanisms in Organic-Rich Shales: Role of Kerogen

Fracture mechanisms in organic-rich shales: role of kerogen

Laurent Brochard[1], Gyorgy Hantal[2], Hadrien Laubie[2], Franz J. Ulm[2] and Roland J.-M. Pellenq[2]

[1]Universit Paris-Est, Laboratoire Navier (UMR 8205), CNRS, ENPC, IFSTTAR, 77455 Marne-la-Valle, France; email: laurent.brochard@enpc.fr
[2]Civil and Environmental Engineering, Massachusetts Institute of Technology, 77 Massachusetts Avenue, Cambridge, MA 02139, USA; email: ghantal@mit.edu, hlaubie@mit.edu, ulm@mit.edu, pellenq@mit.edu

ABSTRACT

In this work we study role of kerogen in the fracture properties of organic-rich shales, and in particular in the ductility of shales. The presence of kerogen and clays in shale is known to increase the ductility. We propose here a multiscale approach to develop of a fine understanding of shale ductility from the molecular scale. We develop and validate a methodology at the molecular scale that can capture the toughness and ductility of a material. We apply this methodology successfully to a silica polymorph and to a kerogen analog, and we confirm the significant ductility of kerogen. Interestingly the silica-kerogen interface exhibits a similar ductility, which is central for the properties of the heterogeneous shale. Finally, we consider a tentative upscaling considering the pull out phenomenon as a likely mechanism of fracture of the shale.

INTRODUCTION

Organic-rich shales are larges reserves of unconventional hydrocarbons that have become more and more attractive with the increasing price of conventional gas and oil. The potential resources of shale gas are estimated between 50 and 100 years of current world consumption [1], but the recovery of these unconventional hydrocarbons is challenging because of the low intrinsic permeability of those reservoirs. To operate such reservoirs at reasonable costs, the oil industry performs hydraulic fracturing. Hydraulic fracturing consists in creating a network of fractures in the reservoir by injecting a fluid under high pressure [2]. The most important factors that influence the crack propagation in the reservoir are the in situ far field and local stress and the fracture properties of the rocks. A fine understanding of the fracture properties of shales is critical for the reliable modeling of hydraulic fracturing. In this work, we focus on a specific aspect of the fracture properties: how the fracture properties depend on the mineralogy and organic content of the shale? Brittleness indicators have been developed to quantify the level of ductility of the shale [3]: shales containing mostly silica and carbonate tend to be very brittle, i.e., they "shatter", leading to a vast array of small-scale induced fractures providing numerous flow paths. Conversely, shales with a significant content of clay and kerogen tend to be ductile, i.e., they deform instead of shattering, leading to

relatively few induced fractures and providing only limited flow paths. The brittleness of shale is important to decide the appropriate location of the horizontal well and to estimate the productivity of the well.

In this work, we aim at developing a fundamental understanding of the toughness and ductility of shales starting at the molecular scale. The characteristic size of the elementary constituents of shales (minerals and kerogen) is as small as a micrometer. At this scale, the study of fracture properties by laboratory experiments is very challenging. Whereas molecular simulation is a convenient alternative to experiment to study the fracture properties at the nano-scale. Ultimately such an approach would enable to capture finely the impact of organic / clay content, or kerogen type / maturity on the fracture properties of shales. In the first section, we present the methodology we develop to estimate fracture properties by molecular simulation. In the second section, we apply this methodology to silica, kerogen and their interface. In the third section, we propose to upscale those fracture properties to estimate the fracture properties of the heterogeneous material.

METHODOLOGY

We propose a methodology to estimate fracture properties by molecular simulation [4]. The methodology, based on the energetic theory of fracture mechanics [5, 6, 7], consists in a thermodynamic integration. We consider a bulk material in which we initiate an initial elliptic through crack (see 1). Then, we load the system in the direction orthogonal to the crack until the crack is fully propagated. During the loading we impose the displacement at the top and bottom boundaries, we impose a constant temperature and we compute the derivative $\Sigma = \frac{1}{L_x L_z} \frac{\partial F}{\partial L_y}\Big|_{T,L_x,L_z}$ of the Helmholtz free energy F with respect to the vertical direction L_y, which can be interpreted as the average stress at the top and bottom boundaries. To compute Σ, we use the virial equation [8]. This procedures corresponds to a loading of the crack in mode I, but can be easily adapted to a loading in mode II by applying a shear instead of a tension. According to the energetic theory of fracture mechanics, the Helmholtz free energy F can take the form of mechanical energy P due to the strain $\underline{\underline{\epsilon}}(\mathbf{r})$ and stress $\underline{\underline{\sigma}}(\mathbf{r})$ over the volume Ω of the solid, i.e., $P = \int_\Omega \left(\int_0^{\underline{\underline{\epsilon}}(\mathbf{r})} \right) \underline{\underline{\sigma}} : d\underline{\underline{\epsilon}} \mathbf{dr}$, and can be released during crack propagation, the critical energy release rate G_c being the corresponding energy released per unit area of crack propagated. Assuming that no other form of energy transformation occur during the loading of the system, the energy balance of the system is: $dF = dP + G_c dA$, where A is the crack area.

At the beginning of the procedure, the system is free of stress and the mechanical energy P is zero. Once we start to increase the loading, the system stores mechanical energy but the crack does not propagate due to insufficient stress intensity at the crack tip. When the loading is large enough, the crack starts to propagate and the mechanical energy stored is released during the propagation. At the end of the procedure the crack is fully propagated over all the system and the mechanical energy stored is again zero since the stress in the system is free of stress. Therefore integrating the curve $\Sigma(L_y)$ over the whole process provides an estimation of the critical energy release rate G_c:

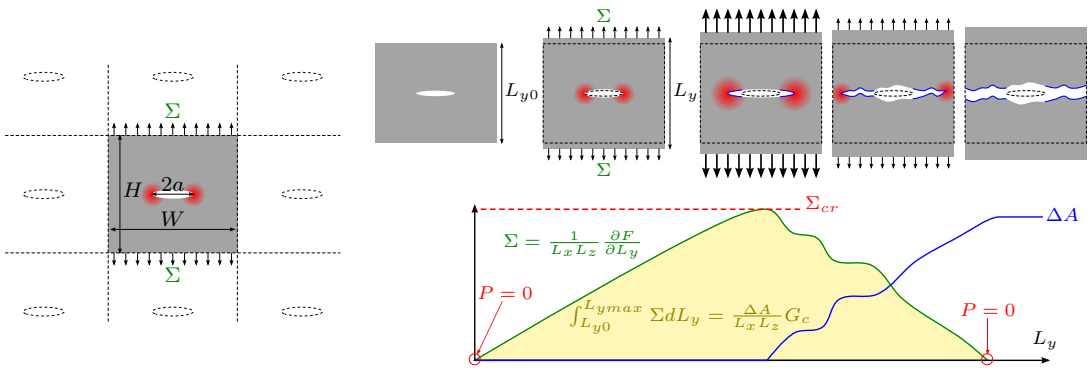

Figure 1. Schematic representation of the proposed methodology.

$$G_c = \frac{L_x L_z}{\Delta A} \int_{L_{y0}}^{L_{ymax}} \Sigma dL_y \tag{1}$$

where ΔA is the total area of crack created. The thermodynamic integration we propose is not limited to linear elastic materials but is valid whatever the mechanical behavior and whatever the fracture properties (brittle or ductile), under two important assumptions: 1 - the crack propagation is assumed in isothermal conditions, 2 - the irreversible processes that occur during the loading are related to the crack propagation and no other form of dissipation take place, e.g., plasticity not related with the crack propagation.

The first assumption, isothermal conditions, is valid if the heat conductivity of the material is large enough. For, the second assumption, cracks with large aspect ratios ensure a sufficient stress singularity at the crack tip and we did not observe any other form of dissipation in all the systems we simulated. In addition to those two assumptions, special care has to be taken on a few aspects [4]: size of the system, the inter-atomic energy potential, and overlap at the periodic boundary conditions.

As an alternative to the thermodynamic integration, one can also consider the usual Linear Elastic Fracture Mechanics (LEFM) to derive the critical stress intensity K_{Ic}, also called toughness, from the maximum average stress Σ_{cr} at the onset of crack propagation 1. According to LEFM, the toughness and the critical stress are linearly related [7]:

$$K_{Ic} = \Sigma_{cr}\sqrt{\pi a} C = \Sigma_{cr}\sqrt{\pi a_{eff}} \tag{2}$$

where $a_{eff} = aC^2$ and the coefficient C is a parameter that depend on the geometry, e.g., C equals 1 for a single crack in an infinite medium. For the doubly periodic geometry we consider, C is a function of a/W and H/W, where the geometrical parameters a, W, and H are defined in Figure 1. We used the pseudo-traction method proposed by Karihaloo et al. [9, 10] to compute numerically the coefficient $C\left(a/W, H/W\right)$ for all the systems we considered.

Using Equation 2 we can derive the toughness K_{Ic} from the critical stress Σ_{cr}, and the toughness is related to the critical energy release rate G_c according to Irwin's formula. For an isotropic material in plane strain [6], which is the case of kerogen in the

next section, we have $G_c = \frac{1-\nu^2}{E} \left(K_{Ic}\right)^2$, where E is the Young's modulus and ν is the Poisson's ratio. For an anisotropic material, which is the case of the silica we consider in the next section, the Irwin's formula is more complex and depends on the different components of the elasticity tensor (see [11]).

For a linear elastic brittle material, the two approaches, i.e., thermodynamic integration and LEFM, are equivalent. However, when a material exhibits a significant ductility, e.g. due to a large plastic zone around the crack tip, the results of the two approaches differ: LEFM is not valid and underestimates the toughness whereas the thermodynamic integration is valid and lead to the actual critical energy release rate.

APPLICATION TO SILICA, KEROGEN AND THEIR INTERFACE

In this section, we apply the methodology presented in the previous section to two of the most common materials in shale: silica and kerogen. In addition, we apply the methodology to molecular reconstructions of the silica-kerogen interface. Silica is a good benchmark for the approach we propose because its mechanical behavior is linear elastic and its fracture behavior is brittle. Therefore, both LEFM and the thermodynamic integration are valid for this material. In addition, many experimental results are available for silica. In contrast, kerogen is known to increase the ductility of shale and, accordingly, we expect to identify this ductile behavior by comparing the results of LEFM and thermodynamic integration.

We considered α-cristobalite [12], a silica crystal metastable at ambient temperature and pressure. We use this specific silica, because the tetrahedral lattice of α-cristobalite adapts very well to the lattice of the molecular representation of kerogen we use, which is key for the simulation of the silica-kerogen interface. For kerogen, we consider a molecular representation of microporous carbon, CS1000, representative of the matrix of a mature kerogen without mesopores [13]. The reactive energy potential we use is reaxFF [14] adapted to systems made of silicon, oxygen, carbon and hydrogen atoms [15, 16].

For both α-cristobalite and CS1000, we performed the loading procedure over many systems with various sizes and various crack lengths, and varying the orientation of the crack in the case of α-cristobalite which is anisotropic. We simulated a total of 33 systems for α-cristobalite and 25 systems for CS1000 [4]. We display in Figure 2 the resulting L_y-Σ curve for three of those systems, one for α-cristobalite with the crack in the (001) plane, a second one for α-cristobalite with the crack in the (100) plane (equivalent to the (010) plane by symmetry) and one for CS1000. The two curves for $alpha$-cristobalite cannot be compared quantitatively since the initiation of the crack is dependent on the geometry which is not the same between those two systems. But in both case the behavior is linear and brittle with a sudden propagation of the crack and a sharp drop of the average stress. By contrast, the behavior of CS1000 is much more ductile with a progressive decrease of the average stress during crack propagation.

We performed the thermodynamic integration for all the systems and we computed the critical energy release rates of CS1000 and α-cristobalite for which we distinguished between the crack propagation in the (001) plane and the propagation in the (100) plane. The results for α-cristobalite were almost independent on the crack orien-

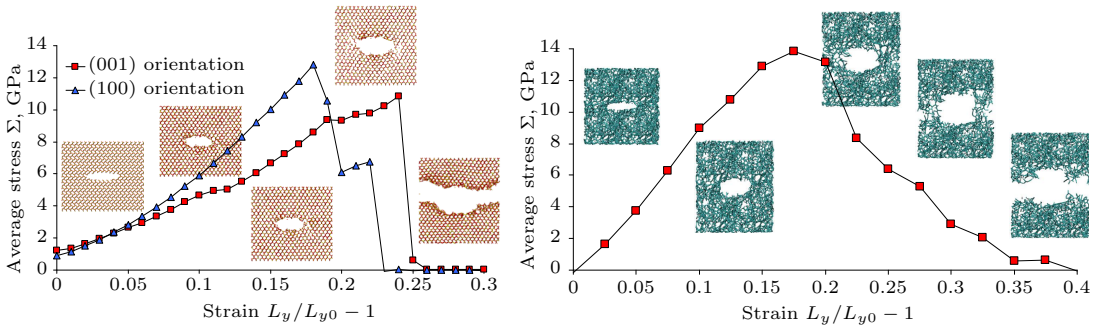

Figure 2. Example of loading curves $\Sigma = \Sigma(L_y)$ for α-cristobalite (left) and CS1000 (right).

tation, crack length and size of the system (Fig. 3). However, the results for CS1000 exhibited a clear correlation with the area of crack created (Fig. 3). We attributed this trend to the overlap of the process zone at the periodic boundary. Indeed, the process zone at the crack tip is important in the case CS1000 whereas it is non-significant for α-cristobalite. A tentative estimate of the size of the process zone is the size r_{pl} of the "plastic region" around the crack tip assuming a plastic behavior of the material. We consider the Dugdale-Barenblatt estimate: $r_{pl} = (\pi/8) \times (K_I/\sigma_{pl})$, where σ_{pl} is the plastic yield stress of the material. We estimated $\sigma_{pl} = 35$ GPa for α-cristobalite and $\sigma_{pl} = 19$ GPa for CS1000. Therefore we have $r_{pl} = 3.38$ Å for α-cristobalite and $r_{pl} = 19.9$ Å for CS1000. This size of the process zone is very small for α-cristobalite compared to the typical size of the system we considered (≈ 70 Å) and, accordingly, it is reasonable to neglect any overlap of the process zone at the periodic boundary. However, for CS1000 the overlap cannot be neglected. As a first order correction for this overlap we considered an effective crack area created $\Delta A_{eff} = \Delta A - L_z r_{pl}/2$ instead of the actual crack area ΔA in the integration Eq. 1. In Figure 3 we display the corrected results and no trend can be identified.

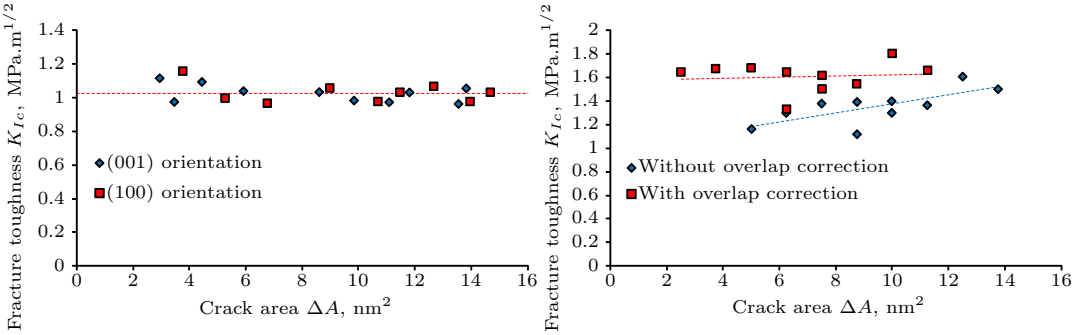

Figure 3. Toughness estimated from thermodynamic integration for α-cristobalite (left) and CS1000 (right).

According to LEFM, the critical stress $\Sigma_c r$ is inversely proportional to $\sqrt{\pi a_{eff}}$ (see Eq. 2). This relation is well verified for α-cristobalite but less accurate for CS1000 (see Fig. 4). We fitted the value of the toughness K_{Ic} (lines in Figure 4) and we compare those values to that obtained previously by thermodynamic integration in Table 1. In Table 1 we converted the critical energy release rates into toughness using the Irwin's Formula for CS1000 (isotropic) and its derivative for α-cristobalite (orthotropic) [11].

We simulated bulk CS1000 to estimate its Young's modulus and Poisson's ratio. For α-cristobalite, we used the elastic tensor measured experimentally [17]. In addition, we include in Table 1 the average toughness measured experimentally for silica [18].

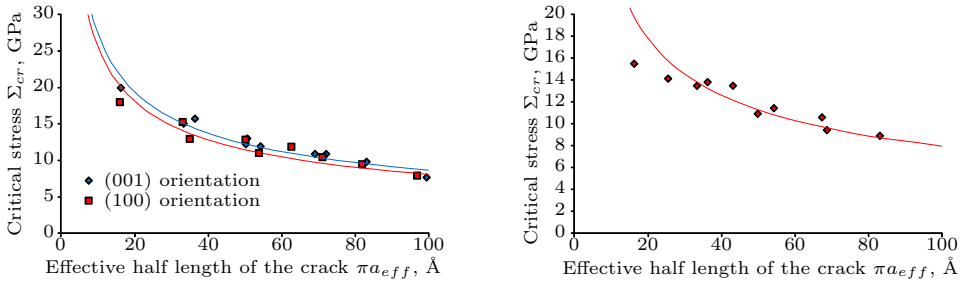

Figure 4. Fit of the critical stress by LEFM for α-cristobalite (left) and CS1000 (right).

For α-cristobalite, the results obtained by thermodynamic integration, derived from LEFM and measured experimentally are very consistent. Accordingly, the methodology we propose works well for this example which is a linear elastic brittle material. For CS1000, however, the results of thermodynamic integration are significantly higher than the results derived from LEFM. This difference is due to the important ductility of this microporous carbon that is readily visible in Figure 2. LEFM is not valid when the material experiences a significant ductility at the scale of the system and leads to an underestimation of the toughness. The thermodynamic integration however is valid even when the material exhibits a significant ductility. Therefore, the value obtained by thermodynamic integration can be regarded as the actual toughness of CS1000. The toughness of CS1000 is much higher than that of silica, but this conclusion is specific to CS1000 and cannot be generalized to kerogen. Indeed, CS1000 is representative of a high density mature kerogen without its mesopores, and accordingly its toughness is in the upper range of what can be expected for kerogen. The ductility of CS1000, however, is an intrinsic property of the microporous carbon which is transferable to kerogen. This is consistent with macroscopic observations: laboratory experiments available in the literature have shown that a significant organic content in shale increases the ductility of shale, but not necessarily the toughness [19, 20].

The fracture properties of a heterogeneous material depends on the fracture properties of the its elementary constituents but also on the fracture properties of the interfaces between those constituents. The crack propagation often occurs at interfaces which have a weaker resistance to fracture. In a previous work [21], we developed a methodology to reconstruct molecular models of silica-kerogen interfaces and we applied this methodology to generate a series of 11 interfaces between CS1000 and α-cristobalite assuming an average situation in terms of kerogen type and maturity. We then applied the mode I loading to these interfaces (see Fig. 5) and estimated the critical energy release rate by thermodynamic integration. For a crack lying at an interface, the theoretical stress field near the crack tip is oscillatory because of the mismatch between the elastic properties of the two materials. As a consequence, the toughness is a combination of the mode I and mode II stress intensities and to convert the critical energy release rate into toughness, one has to consider an alternative formulation of the

Table 1. Summary of the toughnesses estimated by thermodynamic integration, derived from LEFM and measured experimentally

Estimate / measure	K_{Ic}, MPa.m$^{1/2}$	Standard deviation, MPa.m$^{1/2}$
α-cristobalite		
Thermodynamic integration, (001) orientation	1.027	0.053
Thermodynamic integration, (100) orientation	1.027	0.060
LEFM, (001) orientation	0.867	0.056
LEFM, (100) orientation	0.810	0.074
Experimental measurements	0.818	0.070
CS1000		
Thermodynamic integration	1.608	0.127
LEFM	0.797	0.099
Interface between CS1000 and α-cristobalite		
Thermodynamic integration	0.573	0.036
LEFM	0.263	0.029

Irwin's formula [6, 22]. Thus we could estimate the toughness of the interface (see Tab. 1). We also derived the toughness from LEFM as we did for pure CS1000 and pure α-cristobalite. In theory, this approach by LEFM is derived for homogeneous materials and is not strictly exact for interface cracks. But we used this approach to have a basis of comparison with the results from thermodynamic integration and therefore quantify the ductility of the interface.

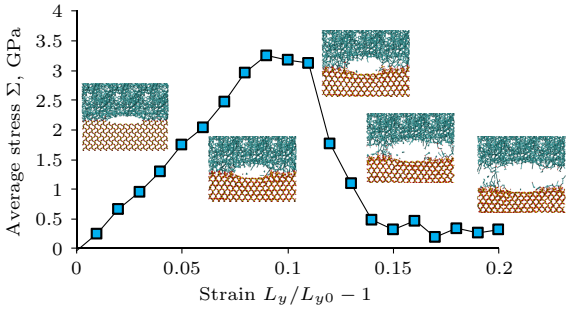

Figure 5. Example of loading curve $\Sigma = \Sigma(L_y)$ for the interface

The strain-stress curve for the interface system (Fig. 5) exhibits clearly some ductility like CS1000 (Fig. 2). This conclusion is supported by the discrepancy between the toughness estimated by thermodynamic integration and that derived from LEFM (Tab. 1). The critical energy release rate of a perfectly brittle material is equal to two times the surface energy γ. Therefore, a possible quantification of the ductility d is the ratio between the critical energy release rate and the surface energy: $d = G_c/\gamma$. $d = 1$ corresponds to a perfectly brittle material, and $d \to +\infty$ corresponds to a perfectly ductile material. Here, for sake of simplicity we assume that the energy release rate derive from LEFM corresponds to the perfectly brittle material: $G_c^{LEFM} = 2\gamma$. Therefore, we have $d = G_c^{thermo}/G_c^{LEFM} = \left(K_{Ic}^{thermo}/K_{Ic}^{LEFM}\right)^2$. With this definition of ductility, we have $d = 1.40$ and $d = 1.61$ for α-cristobalite with the crack orientations (001) and (100), respectively; we have $d = 4.07$ for CS1000; and $d = 4.75$ for the interface. According to this tentative quantification of ductility, the interface is as ductile as the CS1000 itself.

EFFECTIVE FRACTURE PROPERTIES OF HETEROGENEOUS SHALE

In the previous section, we have shown that kerogen exhibits a significant ductility and therefore can turn a brittle shale into a ductile material. However, how the fracture properties of the different constituents of shale combines in the heterogeneous medium needs to be investigated. In particular, the kerogen content is usually small ($\approx 5\%$) and therefore it is not straightforward that such a small content can significantly affect the ductility of the shale. The presence of clay also increases the ductility of shale. We propose here an approach to upscale the fracture properties of shale assuming the shale as a heterogenous material made of a brittle matrix with ductile inclusions. We apply this approach to the specific case of kerogen inclusion in a silica matrix with the results of the previous section. But this upscaling could be adapted to account for clay as the ductile inclusions or for carbonate as the brittle matrix, as long as the clay content remains small ($< 20\%$).

The crack propagation in a heterogeneous material is subject to various unusual phenomena such as crack deflections [23, 24, 25, 26], front roughening [27], trapping [28, 29], bridging [30, 31, 32, 33], particle pull out [30, 31, 34], micro-crack toughening [30, 35] or crack pinning [36, 37]. All these phenomena combine and should be accounted for to fully capture the effective properties of the shale. However, a model combining all these phenomena would be far too complex and we decided to focus on a few of those mechanisms that we consider the most relevant in the present situation. When a crack lying in the brittle matrix (silica) approaches a ductile inclusion (kerogen), the crack front tends to deform to account for the heterogeneity of toughness and mechanical properties between the matrix and the inclusion, and then the crack either penetrates the inclusion or is deflected at the interface. According to the works of He and Hutchinson [25], in the specific case of kerogen and silica, the crack is always deflected. Indeed, the ratio between the critical energy release rates $G_c^{Interface}$ and G_c^{CS1000} at the interface and in CS1000, respectively, is 0.143. According to the work of He and Hutchinson, whatever the angle of approach of the crack at the interface, this ratio is smaller than the ratio of energy release rates between the two scenarios deflection and penetration (at least 0.25). Therefore, following the criterion of He and Hutchinson, the crack never penetrates the ductile inclusions but bypasses eventually forming bridges between the two crack faces until the ductile particle is pulled out inside the crack space. Therefore, we focused our investigation on the particle pull out mechanism which is known to significantly affect the fracture properties of heterogeneous materials. We neglected the front roughening and crack trapping since the impact of these phenomena on the fracture properties is second order compared to the effect of the particle pull-out.

We considered the model of Bower et al. [31] which assumes a periodic distribution of circular bridges in the plane of the crack (Fig. 6). Each inclusion exerts a total force P on the crack faces which depends on the crack opening δ at the location of the inclusion. The model enables to compute the toughness ratio $K_{Ic}^{eff}/K_{Ic}^{matrix}$ of the heterogeneous material with respect to the matrix, in function of the pull-out law $P = P(\delta)$ and of the geometry of the system (R/L, H/L, x_0/L). The key input of this model is the pull-out law $P = P(\delta)$. Bower et al. studied the case of a friction

law which makes sense for the case of fiber reinforced materials. In the present case, we considered an other pull-out law (see Fig. 6) inspired from Figure 5, i.e., representative of the ductility at the kerogen-silica interface. The values of the slope $K_{p.o.}$ and of the critical crack opening $\delta_{p.o}$ can be related to the total energy release during the complete pull-out of the particle. Assuming a spherical inclusion which is pulled-out on half of its surface, we have: $2\pi R^2 G_c^{interface} = \int_0^{2\delta_{p.o}} P(\delta)\, d\delta = K_{p.o.} (\delta_{p.o})^2$. Therefore the values of $K_{p.o.}$ and $\delta_{p.o}$ are constrained by the ratio $K_{Ic}^{interface}/K_{Ic}^{matrix}$. To fully determine the pull-out law a second condition is necessary. As a starting point, we considered an elasticity of the particle pull-out equal to the elasticity of the matrix: $K_{p.o.}^{ref} = (2\pi RE)/(2(1-\nu^2))$, where E and ν are the Young's modulus and Poisson's ratio of the matrix. In the following, we vary the values of $K_{Ic}^{interface}/K_{Ic}^{matrix}$ and $K_{p.o.}/K_{p.o.}^{ref}$.

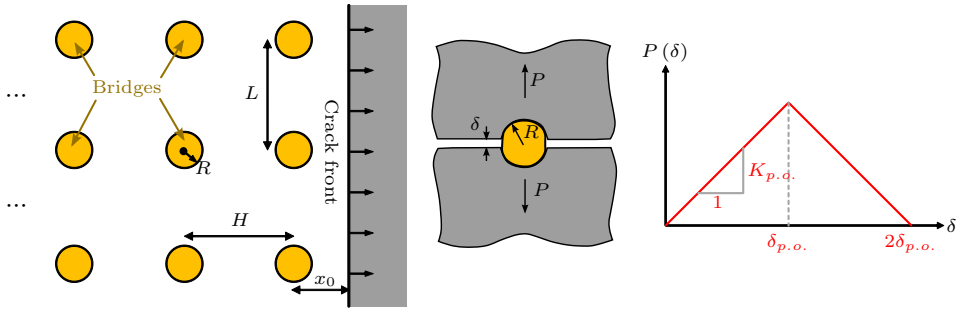

Figure 6. Model considered to represent the pull out phenomenon.

We display in Figure 7 the toughness ratio $K_{Ic}^{eff}/K_{Ic}^{matrix}$ in function of the surface fraction of the inclusions and for various values of $K_{Ic}^{interface}/K_{Ic}^{matrix}$ and $K_{p.o.}/K_{p.o.}^{ref}$. For these calculations, we assumed $H/L = 1$ and $x_0/L = 0.5$. The toughness ratio $K_{Ic}^{eff}/K_{Ic}^{matrix}$ increases with the fraction of inclusion, i.e., the inclusions are toughening the material. The toughening can be very significant, up to a factor of three. This toughening is very sensitive to the interface toughness and to the pull out elasticity. In the case of CS1000 and α-cristobalite $K_{Ic}^{interface}/K_{Ic}^{matrix} \approx 0.7$ and $K_{p.o.}/K_{p.o.}^{ref} \approx 1$. But CS1000 has a higher elasticity than usually admitted for kerogen because the mesopores are not present in this molecular model. The values of elasticity reported in the literature for kerogen correspond more to the curve $K_{p.o.}/K_{p.o.}^{ref} \approx 0.125$. The toughening under those conditions is very significant, more than 2 for a fraction of inclusion of 10% and more than 3 for a fraction of 20%.

As we did in the previous section we can quantify the effective ductility of the heterogeneous material as the ratio between the effective critical energy release rate and the effective surface energy: $d = G_c^{eff}/\gamma^{eff}$. Considering the LEFM estimate of the previous section as estimate of the interface energy, we can compute the ductility d. We obtain a ductility of 1.61 for a surface fraction of ductile inclusions of 0% (pure silica), 9.97 for a surface fraction of 10% and 22.6 for a surface fraction of 20%. Therefore the presence of ductile inclusions in shale may increase dramatically the ductility of the rock.

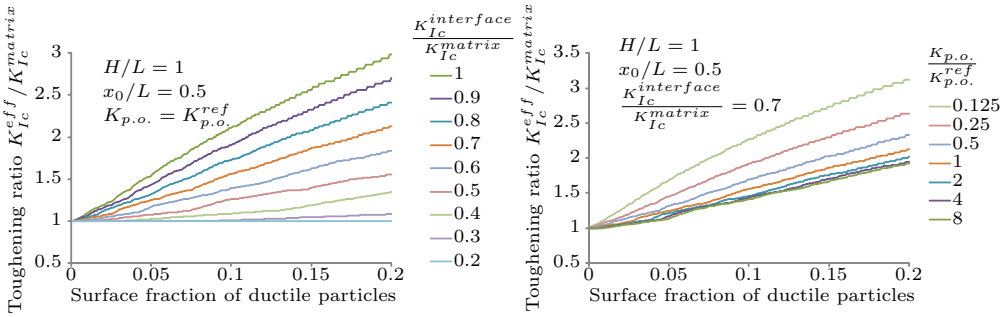

Figure 7. Toughening ratio in function of the various parameters of the problem.

CONCLUSION

In this work, we present a comprehensive approach to study the ductility of organic-rich shales starting at the molecular level and upscaling to the scale of the heterogeneous medium. We develop a methodology to capture the toughness and the ductility by molecular simulation, and apply it to a series of molecular systems representing a silica polymorph, a typical microporous carbon, representative of kerogen, and their interface. We validate the approach by comparing our results with experimental results and with predictions from LEFM valid for linear elastic brittle materials like silica. The kerogen analog and its interface with silica exhibit a significant ductility. Considering an upscaling scenario based on the pull out phenomenon, we perform a tentative upscaling to understand how the presence of ductile inclusions in shale can increase the ductility of the heterogeneous material. We apply this upscaling approach to the case of silica and kerogen and show that the ductility of shale can increase tremendously.

REFERENCES

Kuuskraa, V. et al. (2011) *World shale gas resources,* US EIA, Washington DC.

Birol, F. et al. (2012) *Golden Rules for a Golden Age of Gas,* IEA.

Rickman, R. et al. (2008) *SPE,* 115258-MS.

Brochard, L. et al. (2013) "Fracture Toughness Calculation by Molecular Simulation: Cases of Silica, Microporous Carbons and their Interface." *in preparation.*

Griffith, A. A. (1921) *Philos Tr R Soc S-A,* 221, 163-198.

Leblond, J.-B. (2003) *Mcanique de la rupture fragile et ductile,* Herms Science.

Anderson, T. L. (2005) *Fracture Mechanics,* CRC Press.

Allen, M. P. and Tildesley, D. J. (1989) "Computer Simulation of Liquids." *Oxford University Press.*

Karihaloo, B. et al. (1996) *JMPS,* 44, 1565-1586.

Karihaloo, B. and Wang, J. (1997) *Mech Mater,* 26, 209-212.

Sih, G. C. et al. (1965) *Int J Fracture,* 1, 189-203.

Downs, R. T. and Palmer, D. C. (1994) *Am Mineral,* 79, 9-14.

Jain, S. K. et al. (2006) *Langmuir,* 22, 9942-9948.

van Duin, A. C. T. et al. (2001) *J Phys Chem A,* 105, 9396-9409.

van Duin, A. C. T. et al. (2003) *J Phys Chem A,* 107, 3803-3811.

Chenoweth, K. et al. (2005) *J Am Chem Soc,* 127, 7192-7202.

Yeganeh-Haeri, A. et al. (1992) *Science,* 257, 650-652.

Lucas, J. et al. (1995) *Scripta Metall Mater,* 32, 743-748.

Schmidt, R. A. (1977) *ARMA*, 77-0082.

Slatt, R. M. and Abousleiman, Y. (2011) *The Leading Edge,* 30, 274-282.

Hantal, G. et al. (2013) "Chemistry and molecular reconstruction of kerogen-silica interfaces." *in preparation.*

Rice, J. R. (1988) *J. Appl. Mech.,* ASME, 55, 98-103.

Faber, K. and Evans, A. (1983) *Acta Metallurgica,* 31, 565-576.

Faber, K. and Evans, A. (1983) *Acta Metallurgica,* 31, 577-584.

He, M.-Y. and Hutchinson, J. W. (1989) *Int J Solids Struct,* 25, 1053-1067.

Parmigiani, J. and Thouless, M. (2006) *JMPS,* 54, 266-287.

Rice, J. R. (1985) *J Appl Mech,* 52, 571-579.

Gao, H. and Rice, J. R.(1989) *J Appl Mech,* 56, 828-836.

Mower, T. M. and Argon, A. S. (1995) *Mech Mater,* 19, 343-364.

Evans, A. G. (1990) *J Am Ceram Soc,* 73, 187-206.

Bower, A. and Ortiz, M. (1991) *JMPS,* 39, 815-858.

Swanson, P. L. et al. (1987) *J Am Ceram Soc,* 70, 279-289.

Mai, Y.-W. and Lawn, B. R. (1987) *J Am Ceram Soc,* 70, 289-294.

Hing, P. and Groves, G. (1972) *J Mater Sci,* 7, 427-434.

Shum, D. K. and Hutchinson, J. W. (1990) *Mech Mater,* 9, 83-91.

Daguier, P. et al. (1997) *Phys. Rev. Lett.,* 78, 1062-1065.

Roux, S. et al. (2003) *Eur J Mech A-Solid,* 22, 743-749.